Two-Dimensional Kinetic Analysis Suggests Nonsequential Gating of Mechanosensitive Channels in *Xenopus* Oocytes

Ziv Gil,* Karl L. Magleby,† and Shai D. Silberberg*
*Department of Life Sciences and the Zlotowski Center for Neuroscience, Ben-Gurion University of the Negev, Beer Sheva, 84105 Israel and †Department of Physiology and Biophysics, University of Miami School of Medicine, Miami, Florida 33101 USA

ABSTRACT *Xenopus* oocytes express mechanosensitive (MS_{XO}) channels that can be studied in excised patches of membrane with the patch-clamp technique. This study examines the steady-state kinetic gating properties of MS_{XO} channels using detailed single-channel analysis. The open and closed one-dimensional dwell-time distributions were described by the sums of 2–3 open and 5–7 closed exponential components, respectively, indicating that the channels enter at least 2–3 open and 5–7 closed kinetic states during gating. Dependency plots revealed that the durations of adjacent open and closed intervals were correlated, indicating two or more gateway states in the gating mechanism for MS channels. Maximum likelihood fitting of two-dimensional dwell-time distributions to both generic and specific models was used to examine gating mechanism and rank models. A kinetic scheme with five closed and five open states, in which each closed state could make a direct transition to an open state (two-tiered model) could account for the major features of the single-channel data. Two-tiered models that allowed direct transitions to subconductance open states in addition to the fully open state were also consistent with multiple gateway states. Thus, the gating mechanism of MS_{XO} channels differs from the sequential (linear) gating mechanisms considered for MS channels in bacteria, chick skeletal muscle, and *Necturus* proximal tubule.

INTRODUCTION

Mechanosensitive (MS) channels, which convert mechanical stimuli into electrical responses, have been identified in the three arms of the phylogenetic domain: Eukarya, Eubacteria, and Archaea (Guharay and Sachs, 1984; Sukharev et al., 1994; Le Dain et al., 1998). Through this transduction process, MS channels play a central role in the senses of touch, hearing, balance, and proprioception, as well as being involved in cell volume regulation (Morris, 1990; Sackin, 1995; Hamill and McBride, 1996; Sachs and Morris, 1998; Oakley et al., 1999).

Because the MS channels involved in sensory perception in higher organisms are less accessible to single-channel recording, much of the current information on the kinetic gating mechanisms of MS channels has been derived from studies on MS channels in isolated cells and single-cell organisms. MS channels were first characterized in tissue-cultured embryonic chick skeletal muscle (Guharay and Sachs, 1984, 1985). Kinetic analysis of the single-channel currents indicated that these channels entered at least one open and three closed states during gating. A sequential (linear) gating mechanism in which transitions through the three closed states were followed by a transition to a single open state could approximate the data. Sequential kinetic schemes have also proven useful to characterize the gating of MS channels from *Xenopus* oocytes (MS_{XO} channels), with three closed and one open state (Yang and Sachs, 1990), MS channels from *Necturus* proximal tubule, with two closed and one open state (Sackin, 1989, 1995), and MS channels from *Escherichia coli*, with one closed state, three subconductance states of 30, 70, and 90% of the open state conductance, and one fully open state (Sukharev et al., 1999a).

The purpose of the present study is to further investigate the gating mechanisms of MS_{XO} channels by examining the detailed single-channel kinetic structure. To this end, we have used one-dimensional (1-D) and two-dimensional (2-D) single-channel analysis techniques with maximum likelihood fitting, as well as analysis of subconductance gating. The 1-D dwell-time distributions of the open and closed intervals indicated that the channels enter at least 2–3 open and 5–7 closed kinetic states during gating. Dependency plots derived from the 2-D dwell-time distributions were dominated by reciprocal relationships between the durations of adjacent open and closed intervals, indicating two or more independent transition pathways between the open and closed states. The observation of correlation between adjacent intervals rules out all sequential (linear) gating mechanisms with a single gateway state. A two-tiered model with five open and five closed states, with each closed state having a direct transition pathway to an open state, could approximate the major features of the single-channel data. Subconductance level analysis of two-tiered models, which allowed direct transitions to subconductance levels as well as the fully open level, also suggested that MS channels gate nonsequentially with more than one gateway state.

Received for publication 2 April 2001 and in final form 15 June 2001.

Address reprint requests to Shai D. Silberberg, Ph.D., Department of Life Sciences, Ben-Gurion University of the Negev, P. O. Box 653, Beer-Sheva 84105, Israel. Tel.: 972-8-6472645; Fax: 972-8-6472890; E-mail: silber@bgumail.bgu.ac.il. Correspondence may be addressed to Shai D. Silberberg, Ziv Gil (gilziv@bgumail.bgu.ac.il), or Karl L. Magleby (kmagleby@miami.edu).

0006-3495/01/10/2082/18 $2.00

METHODS

Oocyte isolation and single-channel recording

The methods used for isolation of oocytes, for single-channel recording, and for data analysis were performed as previously described (Silberberg and

Magleby, 1997). Briefly, adult *Xenopus laevis* frogs were anesthetized by immersion in a solution containing 1.5 g/l ethyl m^A-aminobenzoate (methanesulphonate salt, Tricaine, Sigma, St. Louis, MO) and oocytes were removed as described previously (Stühmer and Parekh, 1995). Stage V-VI oocytes were then enzymatically separated, and used within five days of isolation. The vitelline membrane was removed with forceps from the oocytes immediately before the experiments. Currents were recorded from excised inside-out patches of membrane from *Xenopus* oocytes using the patch-clamp technique (Hamill et al., 1981; Sakmann and Neher, 1995). Patch pipettes were fabricated from borosilicate glass (equivalent to Corning No. 7740; Clark Electromedical Instruments, Reading, UK) and coated with Sylgard 184 (Dow Corning Corp., Midland, MI). All analyzed recordings were from excised patches containing a single MS channel from the oocyte.

Unless otherwise indicated, the pipette solution (extracellular solution) and the bath (intracellular) solution contained (mM): NaCl, 150; *N*-tris(hydroxymethyl)methyl-2-aminoethanesulfonic acid (TES) buffer, 5; and EGTA, 2. All solutions were adjusted to pH 7.0. Current traces were low-pass filtered at 5 kHz (−3 dB), using the integral 4-pole Bessel filter of the Axopatch 200B patch-clamp amplifier (Axon Instruments Inc., Foster City, CA), and stored on VCR tape (Instrutech, Port Washington, NY) for subsequent analysis. During analysis, the data were low-pass filtered at 2 kHz (−3 dB) using an 8-pole Bessel filter (Frequency Devices, Haverhill, MA) reducing the dead time (the duration of an interval that reaches the 50% threshold level) to 90 μs. Experiments were performed at room temperature 19–23°C.

The patch of membrane was stretched by applying negative pressure pneumatically to the back of the pipette through a port on the pipette holder. It is the membrane tension resulting from the pressure rather than the pressure per se that activates MS channels (Gustin et al., 1988; Sokabe et al., 1991). Changes in pressure were produced with an electronic valve system that switched the pipette holder between a pressure reservoir and room air (atmospheric pressure). Changes in pressure are expressed in kPa, where 1.0 kPa = 10.2 cm H_2O.

Sampling, log-binning, and plotting dwell-time distributions for half-amplitude threshold analysis

Two types of analysis were carried out in this study: half-amplitude threshold analysis and subconductance analysis. The following part of the Methods details the half-amplitude analysis and the last paragraph of the Methods details the subconductance analysis.

Single-channel current records were sampled at 100 kHz, durations of open and closed intervals were measured with half-amplitude threshold analysis, and stability plots were constructed as described previously (McManus and Magleby, 1988, 1991). The methods used to log-bin the intervals into 1-D dwell-time distributions, fit the distributions with sums of exponentials using maximum likelihood fitting techniques (intervals less than two dead times were excluded from the fitting), determine the number of significant exponential components with the likelihood ratio test, and generate simulated current records with filtering and noise have been described previously (Blatz and Magleby, 1986a; McManus and Magleby, 1988, 1991). The 1-D dwell-time distributions are plotted with the Sigworth and Sine (1987) transformation, as the square root of the number of intervals per bin with a constant bin width on logarithmic time axis.

Log-binning and plotting 2-D dwell-time distributions for half-amplitude threshold analysis

The theory of 2-D dwell-time distributions can be found in Fredkin et al. (1985), Keller et al. (1990), Colquhoun et al. (1996), and Rothberg et al. (1997). The 2-D dwell-time distributions were generated from the single-channel data as detailed in Rothberg and Magleby (1998), and plotted by extending the Sigworth and Sine (1987) transformation to 2-D dwell-time distributions. Briefly, every open interval and its following (adjacent) closed interval were binned, as well as every closed interval and its following (adjacent) open interval, with the logs of the open and closed interval durations of each pair locating the bin on the y and x axes, respectively. The interval pairs used for plotting the 2-D dwell-time distributions and dependency plots were not corrected for the narrowing of intervals with durations less than two dead times resulting from filtering. For display purposes, the 2-D surface plots were constructed from the 2-D histograms with moving bin averaging to smooth out fluctuations in the data. These same smoothed plots were then used to generate the dependency and the dependency significance plots (see below). Details on the moving bin smoothing are in Rothberg and Magleby (1998). The 2-D surface plots were generated from the smoothed data with the program Surfer (Golden Software, Golden, CO), as detailed in Rothberg and Magleby (1998). The method of maximum likelihood fitting of 2-D dwell-time distributions with sums of 2-D exponential components to estimate the significant numbers of open and closed exponential components is detailed in Rothberg and Magleby (1997).

Dependency plots and dependency significance for half-amplitude threshold analysis

Dependency plots were constructed from the 2-D dwell-time distributions as described in Magleby and Song (1992). The dependency for each bin of open-closed interval pairs with mean durations t_o and t_c is:

$$\text{Dependency}(t_o, t_c) = \frac{N_{obs}(t_o, t_c) - N_{ind}(t_o, t_c)}{N_{ind}(t_o, t_c)} \quad (1)$$

where $N_{obs}(t_o, t_c)$ is the observed number of interval pairs in bin (t_o, t_c), and $N_{ind}(t_o, t_c)$ is the calculated number of interval pairs in bin (t_o, t_c) if adjacent open and closed intervals pair independently (at random). The expected number of interval pairs in bin (t_o, t_c) for independent pairing is:

$$N_{ind}(t_o, t_c) = P(t_o) \cdot P(t_c) \quad (2)$$

where $P(t_o)$ is the probability of an open interval falling in the row of bins with a mean open duration of t_o, and is given by the number of open intervals in row t_o divided by the total number of open intervals, whereas $P(t_c)$ is the probability of a closed interval falling in the column of bins with a mean closed duration of t_c, and is given by the number of closed intervals in column t_c divided by the total number of closed intervals. The significance of the dependencies was estimated using a moving bin paired t test, as described previously (Rothberg and Magleby, 1998).

Estimating the most likely rate constants for kinetic schemes for half-amplitude threshold analysis

The most likely rate constants for the examined kinetic schemes without subconductance levels were determined from fitting the 2-D dwell-time distributions. Fitting was done using an iterative maximum likelihood fitting procedure similar to the one detailed in McManus and Magleby (1991), except that 2-D dwell-time distributions replaced the 1-D dwell-time distributions, and the correction method of Crouzy and Sigworth (1990) for missed events because of filtering replaced our previous correction method. Whereas the interval durations used in the 2-D fitting were corrected for narrowing arising from the filtering, the fitting of the data was typically restricted to intervals with durations greater than two dead times. Additional details of the fitting, including the methods used to correct for missed events using the method described in Crouzy and Sigworth (1990), are given in Rothberg and Magleby (1998). To simplify the writing, the text will refer to the fitting of the (smoothed) 2-D dwell-time distributions (surface plots) presented in the figures, when, in reality, the nonsmoothed

2-D frequency histograms were fitted. Fitting the 2-D frequency histograms was mathematically equivalent to fitting each individual pair of intervals, but much faster (Rothberg et al., 1997).

Evaluating and ranking the kinetic schemes for half-amplitude threshold analysis

Normalized likelihood ratios (NLR) were used to compare the ability of the kinetic schemes to describe the experimental 2-D dwell-time distributions by comparison to the description given by the theoretical best fit (McManus and Magleby, 1991; Rothberg and Magleby, 1998). Normalization takes into account the differences in numbers of interval pairs among experiments so that direct comparisons can be made among channels. The NLR per 1000 interval pairs, NLR_{1000}, is defined as:

$$NLR_{1000} = \exp((\ln S - \ln T)(1000/N)) \quad (3)$$

where ln S is the natural logarithm of the maximum likelihood estimate for the observed 2-D dwell-time distributions given the kinetic scheme, ln T is the natural logarithm of the maximum-likelihood estimate for the theoretical best description of the observed distributions with sums of 2-D exponential components or with generic models (see Results), and N is the total number of fitted interval pairs in the observed dwell-time distributions. The NLR for one interval pair is given by

$$NLR_1 = (NLR_{1000})^{0.001} \quad (4)$$

The NLR_{1000} and NLR_1 can be used to evaluate the error per 1000 interval pairs or one interval pair, respectively, between the examined model and the theoretical best fit. A value of 1.0 for either the NLR_1 or NLR_{1000} indicates that the model describes the data as well as the theoretical best description used for comparison.

Although the NLR gives a measure of how well different kinetic schemes describe the data, it cannot be used directly for ranking schemes, because no penalty is applied for the increased numbers of free parameters. To overcome this difficulty, the Schwarz criterion (Schwarz, 1978) was used to apply penalties and rank models, as detailed in McManus and Magleby (1991). The Schwarz criterion (SC) is given by

$$SC = -\ln S + (0.5\,F)(\ln N) \quad (5)$$

where ln S is the natural logarithm of the maximum likelihood estimate, F is the number of free parameters, and N is the number of interval pairs. The scheme with the smallest SC is ranked highest.

Analysis of subconductance gating

Kinetic analysis of MS_{XO} channel gating was also carried out allowing transitions to subconductance states by using the QUB suite of programs (www.qub.buffalo.edu; Qin et al., 1996, 2000a,b). The amplitude and lifetimes of the fully closed, subconductance, and fully open levels were first estimated and used to generate idealized conductance-level sequences. Then, the most likely rate constants for transitions among the various states in the examined kinetic schemes were determined and the models ranked based on the calculated maximal likelihoods. The kinetic schemes incorporating subconductance states were ranked with Eq. 5, which applies a penalty for extra free parameters. The two methods of analysis used in this paper (50% threshold analysis and subconductance analysis) both had their advantages and disadvantages (see Discussion), while leading to the same conclusion of multiple gateway states in the gating of MS_{XO} channels.

Fitting of single data sets and maintaining detailed balance

Rate constants for kinetic schemes are best estimated by the simultaneous fitting of multiple, stable data sets obtained over a wide range of experimental conditions to constrain the rate constants. This was not done in the present study because, although it was possible to obtain stable data under single sets of experimental conditions, it was difficult to obtain sufficient stable data over a wide range of experimental conditions from any one channel for such simultaneous fitting. Therefore, for this study, only single data sets were fit at any one time. Such fitting of models to single data sets is suitable to determine which of the examined models can be excluded and which are consistent with the gating, and also to rank models, but usually does not constrain the individual rate constants. Consequently, although the rate constants given in the figure legends can describe the data for the given models, as shown in the figures, it would be expected that other sets of rate constants may be able to give equally good descriptions. Although some of the rate constants may be poorly defined, it should be noted that the estimated rate constants are sufficient to determine which classes of gating mechanisms are consistent with the gating and which are not, which is the purpose of this paper. The entire fitting was constrained so that detailed balance (microscopic reversibility) was maintained, and this was also the case for the generic models.

RESULTS

Single-channel currents reveal that MS_{XO} channels have complex gating kinetics

Fig. 1 *A* presents currents recorded from a single MS_{XO} channel activated by stretch in a patch of membrane excised from a *Xenopus* oocyte. The membrane was stretched by applying −7 kPa of pressure to the shank of the patch pipette. From these records it can be seen that the gating of the channel is complex. Channel openings occur typically in bursts separated by brief closed intervals that are orders of magnitude less in duration than the much longer closed intervals separating bursts. In addition to the bursts of many openings, isolated openings also occur. Such apparent groupings of open and closed intervals into classes of different durations would suggest that the channel gates in multiple open and closed states (Colquhoun and Hawkes, 1981, 1982; Magleby and Pallotta, 1983; Colquhoun and Sigworth, 1995).

In addition to the classes of intervals based on duration, there were also classes of intervals based on conductance. Such levels could be observed in expanded single-channel records, as shown in Fig. 9, and in Silberberg and Magleby (1997). The analysis in the initial part of this paper will be restricted to the kinetics of the interval durations measured with half-amplitude threshold analysis (see Methods). On this basis, openings to subconductance levels less than half-amplitude will not be detected, and openings to subconductance levels greater than the half-amplitude level will be classified as open intervals. Such a simplified kinetic analysis is sufficient to characterize the basic features of the gating and distinguish among several different classes of gating mechanism. Kinetic analysis of channel gating that includes transitions to subconductance levels is applied in a later section.

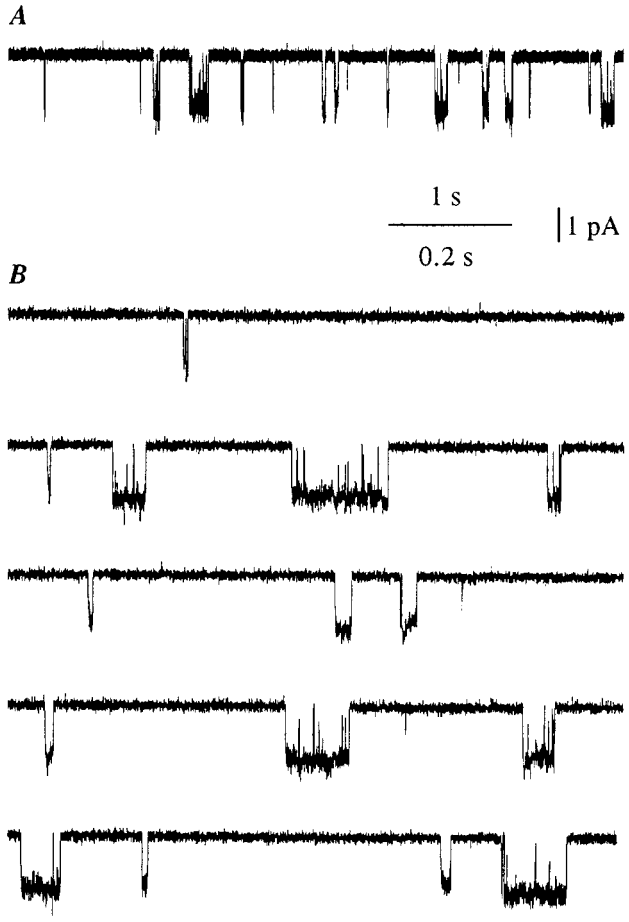

FIGURE 1 Representative current records from an excised membrane patch containing a single MS_{XO} channel. (*A*) Continuous current record from a single MS_{XO} channel activated by pressure in an excised patch of membrane. Downward (inward) currents indicate channel opening. (*B*) Expanded time resolution of the current record shown in *A*. The current record has been cut into five consecutive segments for display. Holding potential −60 mV, pressure −7 kPa. Channel Z100.

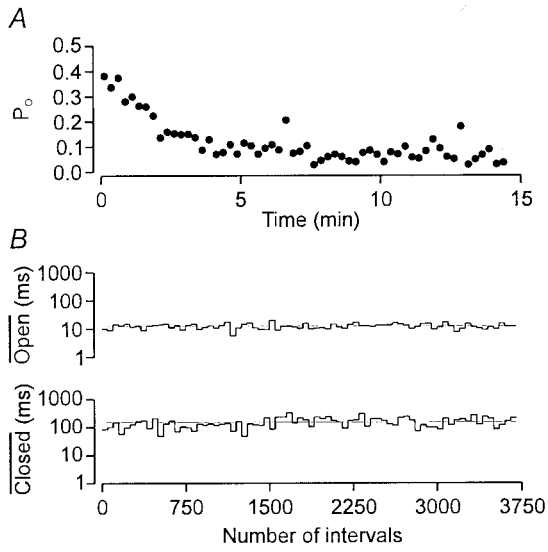

FIGURE 2 Selecting stable data for analysis. (*A*) Open channel probability (P_o) for a single MS_{XO} channel plotted as a function of time after a pressure step. Average P_o decreased from ~0.4 to ~0.07 within 5 min and then remained relatively stable. Each point plots the average P_o over 15 s of continuous channel activity. (*B*) Stability plots of the mean open and mean closed times for 3700 open and 3700 closed events, corresponding to the last ~8 min of activity in *A*. Each bin represents the average duration of 50 consecutive open or closed intervals. The lines through the data correspond to the mean open interval duration (12.1 ms) and the mean closed interval duration (149.4 ms) over the entire data set. Channel Z100.

Gating among 2–3 open and 5–7 closed states

An estimate of the minimal number of kinetic states a channel enters during gating can be obtained from the numbers of significant exponential components required to describe the dwell-time distributions (Colquhoun and Hawkes, 1981, 1982). Such analysis requires that large amounts of stable single-channel data be analyzed, as the ability to resolve components increases with the numbers of intervals (McManus and Magleby, 1988).

An example of how stable data were identified for analysis for the channel examined in Fig. 1 is presented in Fig. 2. The first step toward identifying stable data was to plot the open probability against time after the application of −7 kPa of pressure, as shown in Fig. 2 *A*, where each point plots mean open probability for consecutive 15-s periods. In this example, the open probability, P_o, initially decreased with time, although the applied pressure remained constant, and then approached a relatively stable level of ~0.07. In experiments of this type, a relative stable P_o was often reached several minutes after stepping the pressure. Stability plots were then generated from the data where P_o remained stable. Fig. 2 *B* presents stability plots of the data taken from the last ~8 min of activity in Fig. 2 *A*. The stability plots were constructed by plotting the mean open and the mean closed interval durations for each 50 consecutive intervals, against interval number. The stability of the 3700 open and 3700 closed mean interval durations is readily apparent. The MS_{XO} channels seldom displayed mode shifts, which are a common feature of many ion channels (Patlak et al., 1979; Hess et al., 1984; Patlak and Ortiz, 1985; Blatz and Magleby, 1986b; McManus and Magleby, 1988; Delcour et al., 1993). The slow adaptation to constant pressure in Fig. 2, with a time course of minutes, is considerably slower than a rapid adaptation that has also been observed (Hamill and McBride, 1992). Hence, there may be both fast and slow adaptation of MS channels in oocytes activated by pressure.

Fig. 3 plots open and closed dwell-time distributions for the stable data shown in Fig. 2 *B*. The open distribution (Fig. 3 *A*) could not be fit by a single exponential (*dashed line*) and was best fit with the sums of three significant exponential components (*continuous line*). The closed distribution (Fig. 3 *B*) was best fit with the sums of five significant exponential components. Three significant open and five significant closed exponential components were also obtained with 2-D fitting with

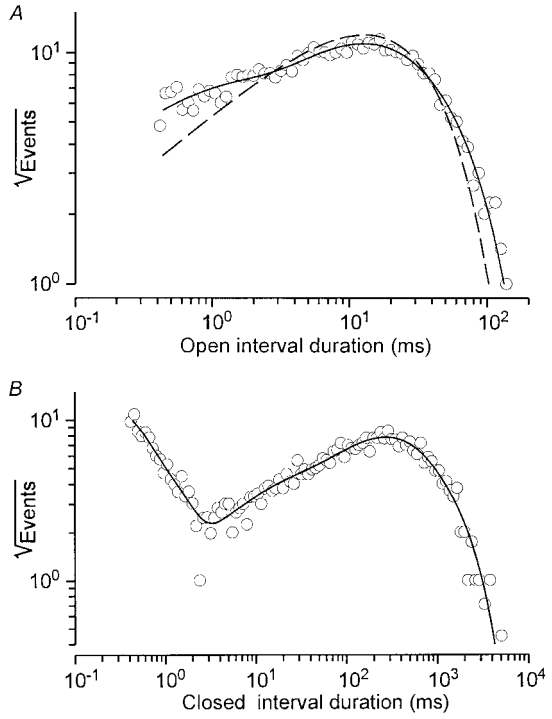

FIGURE 3 MS_{XO} channel gating is complex. Distributions of open (*A*) and closed (*B*) interval durations for the data plotted in Fig. 2 *B* were log-binned at a resolution of 25 bins/decade and plotted as the square-root of the number of intervals in each bin. The solid lines are maximum likelihood fits with sums of exponentials. The open intervals were described by the sum of three significant exponential components ($p < 0.05$) with time constants (and areas) of 0.86 ms (0.16), 9.3 ms (0.39), and 18 ms (0.45). The closed intervals were described by the sum of five significant exponential components ($p < 0.05$) with time constants (and areas) of 0.17 ms (0.60), 0.51 ms (0.11), 18 ms (0.02), 230 ms (0.19), and 550 ms (0.08). The *dashed line* in *A* is the maximum likelihood fit with a single open exponential component. Channel Z100.

sums of 2-D exponential components. These observations suggest that the channel was gating among a minimum of three open and five closed states. In experiments on seven additional stretch activated channels, 2–3 open and 5–7 closed exponential components were detected (details in Table 1), suggesting that MS_{XO} channels gate among a minimum of 2–3 open and 5–7 closed states.

Fig. 4 plots the time constants and magnitudes of the exponential components fitted to the open and closed dwell-time distributions for the eight examined channels. The time constants of the three open components typically ranged over an order of magnitude, whereas the time constants of the five closed components typically ranged over 3–4 orders of magnitude. The areas of the open components generally increased as the time constants increased, whereas the areas of the closed components generally decreased as the time constants increased. Although the trend of the data is generally consistent among channels, some variation in results would be expected because the values of P_o for the eight channels ranged from 0.04 to 0.51.

Kinetic structure of the MS_{XO} channel

To determine what general types of gating mechanisms might be consistent with the observed activity of MS_{XO} channels, we examined the kinetic structure of the channels, which contains information about the connections among the various open and closed states (Magleby and Song, 1992; Rothberg and Magleby, 1998, 1999). The kinetic structure for the channel examined in Figs. 1–3 is presented in Fig. 5. The 2-D dwell-time distribution in Fig. 5 *A* plots how frequently open intervals of the indicated durations occur next (adjacent) to closed intervals of the indicated durations. The log of the durations of each adjacent open and closed interval locate the bin on the *x* and *y* axes, respectively, and the *z* axis plots the square root of the number of observations (interval pairs) per bin (see Methods). The left panel in Fig. 5 plots brief open intervals adjacent to brief closed intervals at the front corner of each plot (designated by position 1), and the right panel in Fig. 5 plots the reverse-angle of the distribution (long open intervals adjacent to long closed intervals at the front corner of each plot, designated by position 6). The most frequently observed interval pairs were the long open intervals adjacent to the brief closed intervals (position 4). The second most frequently observed interval pairs were the long open intervals adjacent to the long

TABLE 1 Experimental conditions, number of open and closed intervals fit, and estimates of the minimal number of kinetic states for MS_{xo} channels

Channel	Holding Potential (mV)	Pressure (kPa)	Solutions NaCl (mM) (in/out)	Number of intervals	P_o	Number of states	
						Open	Closed
Z100 (▽)	−60	−7	150/150	7458	0.07	3	5
Z101 (□)	−60	−6	50/150	13092	0.28	3	5
Z104 (○)	−20	0	50/150	17858	0.07	3	7
Z105 (▲)	−40	0	150/150	10044	0.05	2	5
Z108 (◇)	−40	0	150/150	8834	0.04	2	6
Z112 (*)	−20	0	50/150	16580	0.34	3	5
Z113 (△)	−50	−10	150/150	11894	0.51	3	5
Z114 (■)	−50	−6	150/150	7064	0.1	2	5

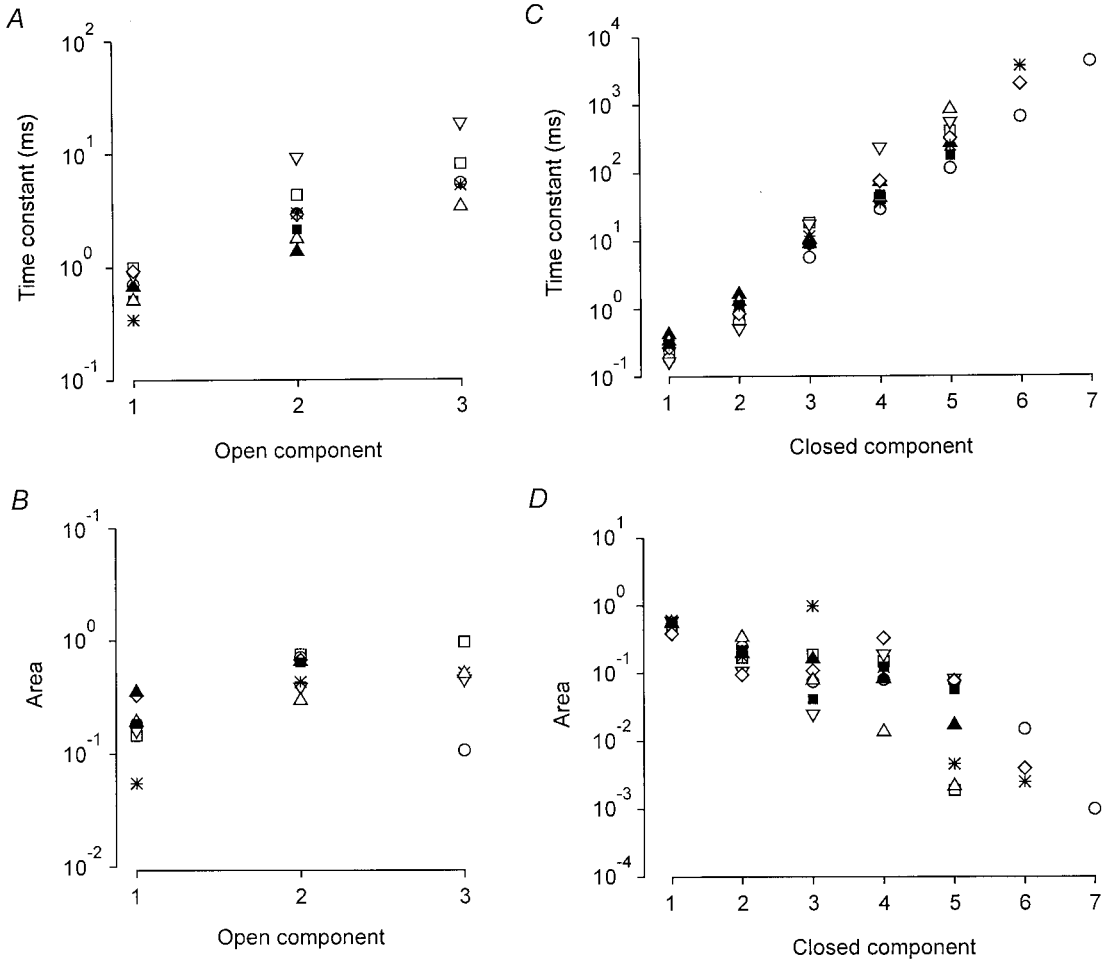

FIGURE 4 MS_{XO} channels gate among a minimum of 2–3 open and 5–7 closed states. Time constants and areas of the open (*A* and *B*) and closed (*C* and *D*) exponential components fit to the 1-D dwell-time distributions for eight different channels. Each MS_{XO} channel is represented by a different symbol, corresponding to the symbols in Table 1.

closed intervals (position 6). The frequencies of the brief open intervals adjacent to the brief, intermediate, and long closed intervals (positions 1, 2, and 3) were less.

Although the 2-D dwell-time distributions give a measure of the relative frequency of occurrence of the various interval pairs, they do not directly indicate which interval pairs occur in excess or deficit of what would be expected for random pairing of the open and closed intervals. Such information gives insight into the connections among the open and closed states (Magleby and Song, 1992). This information is contained in the dependency plots shown in Fig. 5 *B*, *E*, which plot the fractional excess and deficit of interval pairs over that expected for independent pairing of open and closed intervals (see Methods). A dependency of zero (*thick dark lines*) would indicate no excess or deficit of interval pairs when compared with that expected for independent pairing. Dependencies of $+0.5$ or -0.5 would indicate a 50% excess or 50% deficit, respectively, over that expected from independent pairing of interval pairs.

From the two views of the dependency plot it can be seen that brief open intervals adjacent to brief closed intervals occurred ~30% less frequently than would be expected by chance pairing alone (position 1, Fig. 5 *B*), and that long open intervals adjacent to long closed intervals occurred ~25% less frequently than would be expected by chance pairing alone (position 6, Fig. 5 *E*). Such a deficit of interval pairs suggests that the states (or compound states) that generate brief open intervals adjacent to brief closed intervals are not effectively connected, and that the states (or compound states) that generate long open intervals adjacent to long closed intervals are also not effectively connected.

In contrast, long open intervals adjacent to brief closed intervals (position 4) occurred ~35% more frequently than expected by chance pairing alone. This excess of interval pairs suggests that the states (or compound states) that generate long open intervals adjacent to brief closed intervals are effectively connected. A similar case can be made

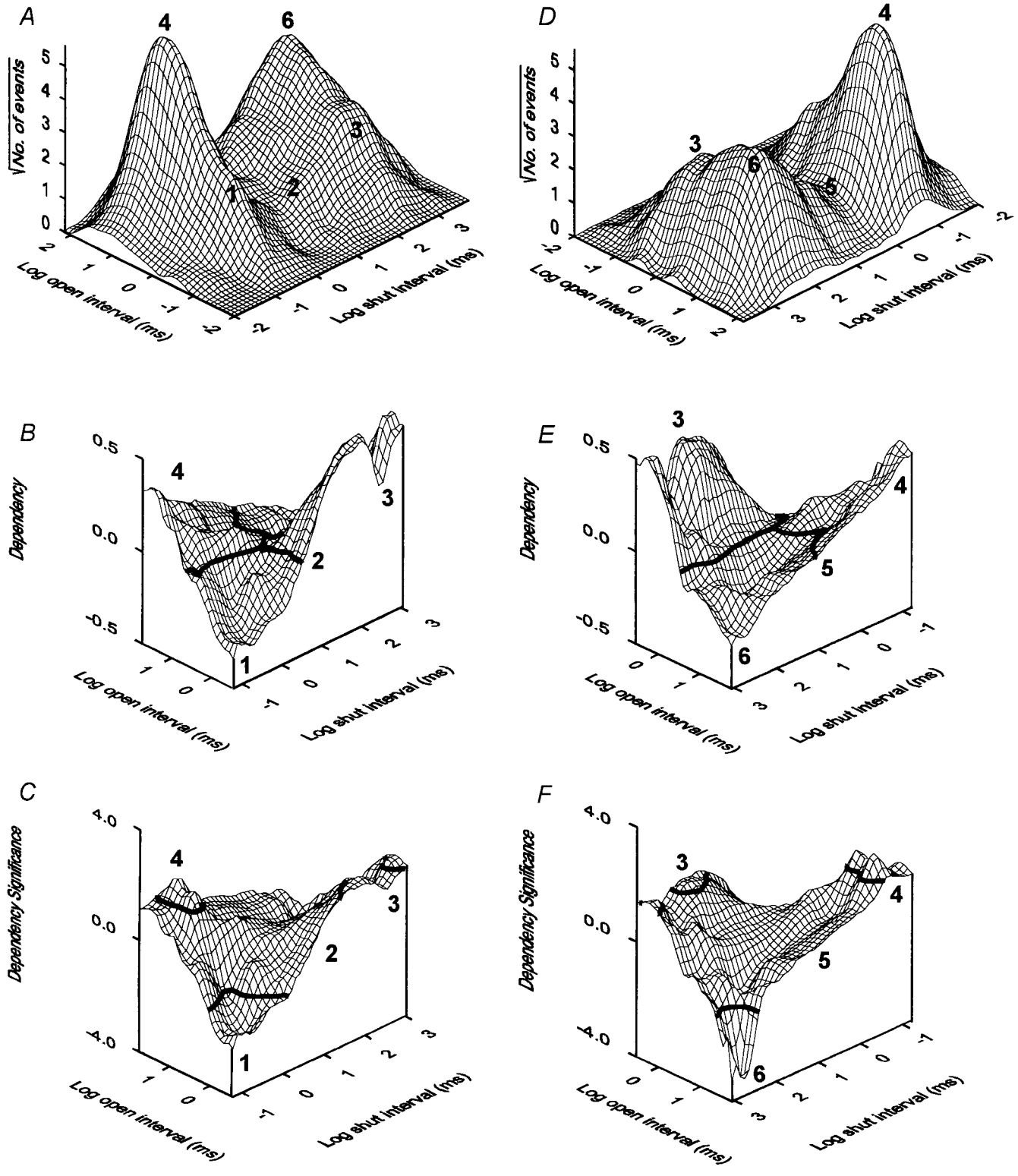

FIGURE 5 2-D analysis of MS_{XO} channel gating reveals at least two gateway states. (*A*) 2-D dwell-time distribution. Adjacent open and closed intervals were binned as pairs, with the logs of the open and closed interval durations locating the bins on the *x* and *y* axes, respectively. The *z* axis plots the square root of the number of intervals in each bin. (*B*) Dependency plot for the data presented in *A*. Dependency indicates the fractional excess or deficit of interval pairs between the observed 2-D dwell time distribution in *A* and the 2-D dwell time distribution calculated assuming independent pairing of open and closed intervals. The *heavy lines* indicate a dependency of zero. (*C*) Dependency significance of the dependency presented in *B*. Dependency significance indicates the log of the *P* value times the sign of the dependency at each bin (see Methods). Absolute values of dependency significance $> \pm 1.3$, depicted by thick lines, indicate significant values ($p < 0.05$). Dependencies at positions 1, 3, 4, and 6 are significant. (*D–F*) Reverse-angle view of the plots in *A–C*, respectively. Channel Z100.

for brief open intervals adjacent to long closed intervals (position 3) that occurred 45% more frequently than expected by chance pairing alone.

Fig. 5 *C*, *F* plot the significance of the dependencies in Fig. 5 *B*, *E*, respectively, as the logarithm of the estimated *P* value, which is then multiplied by the sign of the dependency to indicate whether the paired intervals are in excess or deficit. Values of dependency significance >1.3, 2.0, and 3.0 would indicate $p < 0.05$, 0.01, and 0.001, respectively, for an excess of intervals, and values of dependency significance <−1.3, −2.0, and −3.0 would indicate $p < 0.05$, 0.01, and 0.001, respectively, for a deficit of intervals. The heavy lines on the plots at −1.3 and 1.3 indicate the significance level of $p = 0.05$. The dependencies at positions 1, 3, 4, and 6 are seen to be significant.

For the eight MS_{XO} channels whose kinetic structure was examined in this study (see Table 1), the features of the 2-D dwell-time distributions and also of the dependency plots were similar to those shown in Fig. 5, with visible excesses (positions 3 and 4) or deficits (positions 1 and 6) in dependency occurring for all eight channels. These visually observed dependencies were significant at positions 1 for all eight channels, significant at position 3 for 7 of the 8 channels, and significant at positions 4 and 6 for 6 of the 8 channels.

The observation of significant dependencies indicates two or more gateway states in the underlying kinetic gating mechanism (see Magleby and Song, 1992), where the number of gateway states is given by the number of states that need to be removed to completely sever all transitions between open and closed states (Fredkin et al. 1985; Colquhoun and Hawkes, 1987). Knowing the minimal number of gateway states can give insight into mechanism. For example, gating mechanisms such as C-C-C-O and C-C-O-C, in which C and O represent closed and open states, have a single gateway state, as removing a single state in each scheme can completely sever all connections between open and closed states. In contrast, gating mechanisms such as O-C-C-C-O and C-C-O-C-O have two gateway states.

Sequential gating mechanisms with one gateway state are inconsistent with the gating of MS_{XO} channels

Kinetic gating mechanisms that have been used previously for the gating of MS channels are sequential, with a single gateway state (Guharay and Sachs, 1984, 1985; Yang and Sachs, 1990; Sackin, 1995; Sukharev et al., 1999a). Our observation of significant dependencies (Fig. 5, *B–E*) suggests that such sequential models with a single gateway state would be inconsistent with the gating of MS_{XO} channels. To examine this point further, we tested whether a sequential model with three open and five closed (3/5) states, as given by scheme I, would be able to capture the basic features of the gating.

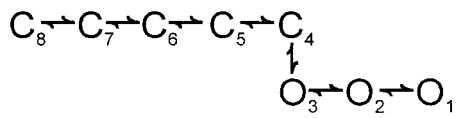

Scheme I

To investigate whether scheme I could account for the kinetic structure, the most likely rate constants for the scheme were estimated by fitting the experimental 2-D dwell-time distributions to find the rate constants that maximized the likelihood that the experimental data were drawn from the 2-D distribution predicted by scheme I (see Methods). These rate constants were then used with scheme I to simulate a single-channel current record with filtering and noise equivalent to that in the experimental data. The simulated current record was then analyzed in the same manner as the experimental current record to generate the predicted 2-D dwell-time distribution and dependency plot shown in Fig. 6 *A* and *B*. Comparison to the experimental data in Fig. 5 *A* shows that although scheme I predicted the general shape of the 2-D dwell-time distribution, the amplitudes of some of the predicted peaks differed from those in the experimental data, most apparently at position 1. Differences in the amplitudes of some of the predicted and experimental peaks in the 2-D dwell-time distribution suggest that scheme I should not describe the dependencies observed in the experimental data. That this is the case can be seen in Fig. 6 *B*, where scheme I predicts a flat dependency plot, with little if any dependence, compared with the significant dependencies in the experimental data (Fig. 5 *B)*. A lack of dependence would be expected for scheme I, because open and closed intervals pair independently for models with a single gateway state. Consequently, there would be no excesses or deficits of interval pairs (Magleby and Song, 1992). We also examined modifications of the sequential model described by scheme I in which the three open states were replaced with one, four, or five open states, and the five closed states were replaced with either one or four closed states. These models also predicted essentially flat dependency plots, as would be expected because of the single gateway state. The lack of dependence in these models when compared with the significant dependence in the experimental data indicates that sequential models with one gateway state can be rejected for the gating of the MS_{XO} channel.

A generic model with three open and five closed states could approximate the steady-state gating of MS_{XO} channels

MS_{XO} channels typically gate in at least three open and five closed states (Table 1). Therefore, we explored whether it

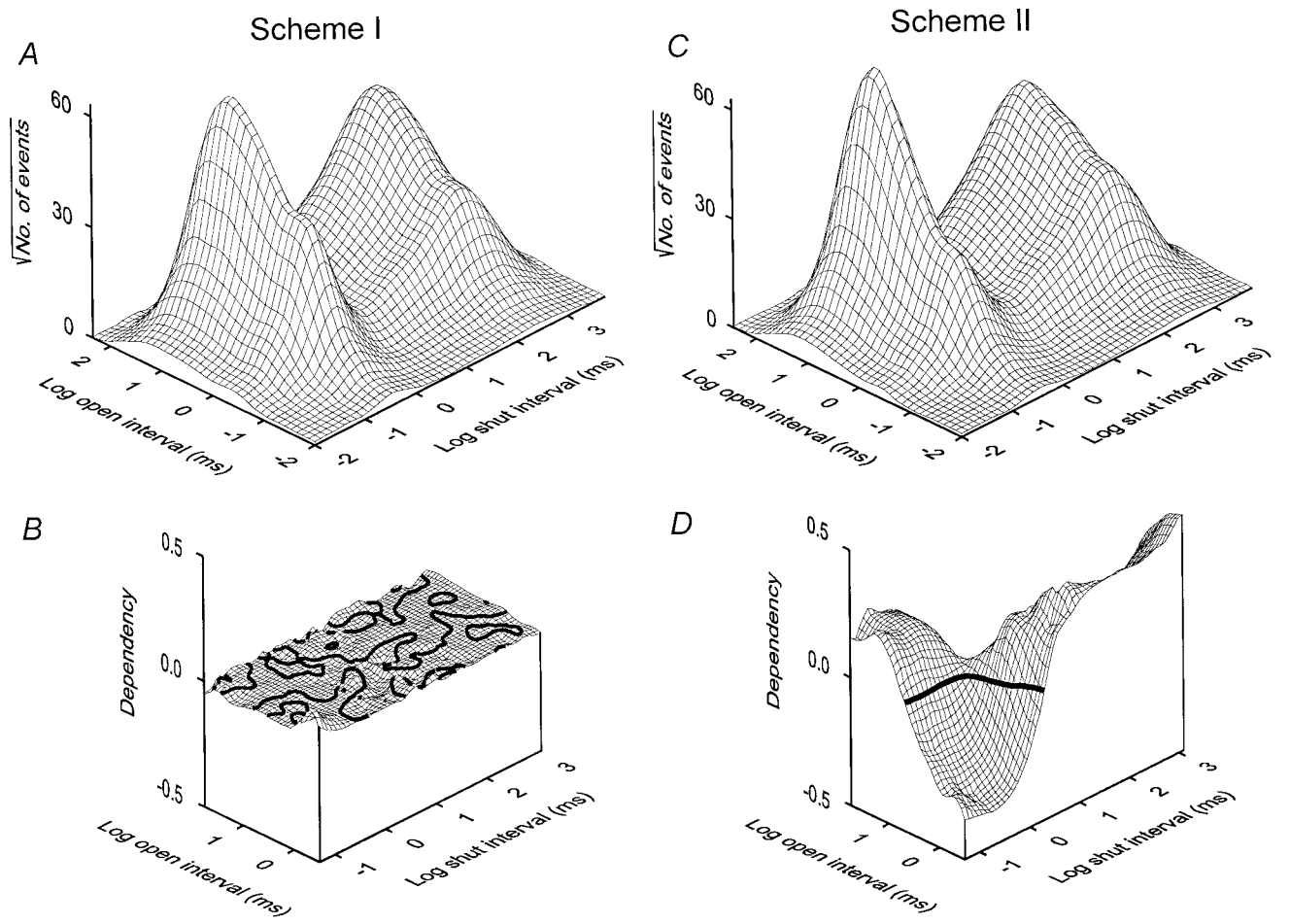

FIGURE 6 A sequential gating scheme with a single gateway state between five closed and three open states cannot account for the kinetic gating structure of MS_{XO} channels. (*A* and *B*) Dwell-time distributions and dependency plots predicted by the linear scheme I. The rate constants used in the prediction were obtained from the maximum likelihood fitting of the 2-D dwell-time distribution in Fig. 5 *A*. (*C* and *D*) Dwell-time distributions and dependency plots predicted by the generic scheme II. The *heavy lines* in *B* and *D* indicate a dependency of zero. The linear scheme I predicts a flat dependency, in contrast to the significant dependencies in the experimental data (Fig. 5 *B*). The generic scheme II captures the features of the experimental data. The rate constants for scheme I were (s^{-1}): k12, 198.5; k21, 145.3; k23, 641.1; k32, 2873; k34, 1674; k43, 5078; k45, 1975; k54, 405.6; k56, 1784; k65, 65.72; k67, 44.68; k76, 35.67; k78, 0.8570; k87, 2.587. Rate constants are not listed for the generic model, as they have no direct physical meaning. Channel Z100.

might be possible to find a kinetic scheme with three open and five closed states (3/5) that would describe the experimental data. Because it is not practical to test all possible specific schemes with three open and five closed states, we first examined whether an uncoupled generic scheme that would be equivalent to all specific schemes with three open and five closed states could describe the data. Because the generic scheme was equivalent to all specific schemes with three open and five closed states, then it would also be equivalent to the most likely specific schemes with three open and five closed states. This approach is described in Rothberg and Magleby (1998), and is based on the theoretical work of Kienker (1989), who showed that uncoupled schemes are mathematically equivalent to all schemes with the same numbers of open and closed states.

The uncoupled generic scheme that was tested is given by scheme II, where all open states make direct connections to all closed states. The scheme is said to be uncoupled because there are no direct transition pathways from one open state to another open state or from one closed state to another closed state. We examined whether scheme II could account for the data by solving for the most likely rate constants for scheme II by fitting the 2-D dwell-time distribution. Using these rate constants with scheme II, we then simulated single-channel data to predict the 2-D dwell-time distribution and dependency plot. Comparison of the predicted results in Fig. 6 *C*, *D* to the experimental data in Fig. 5 *A*, *B*, shows that scheme II approximated the kinetic structure of the gating. Thus, one or more specific schemes with three

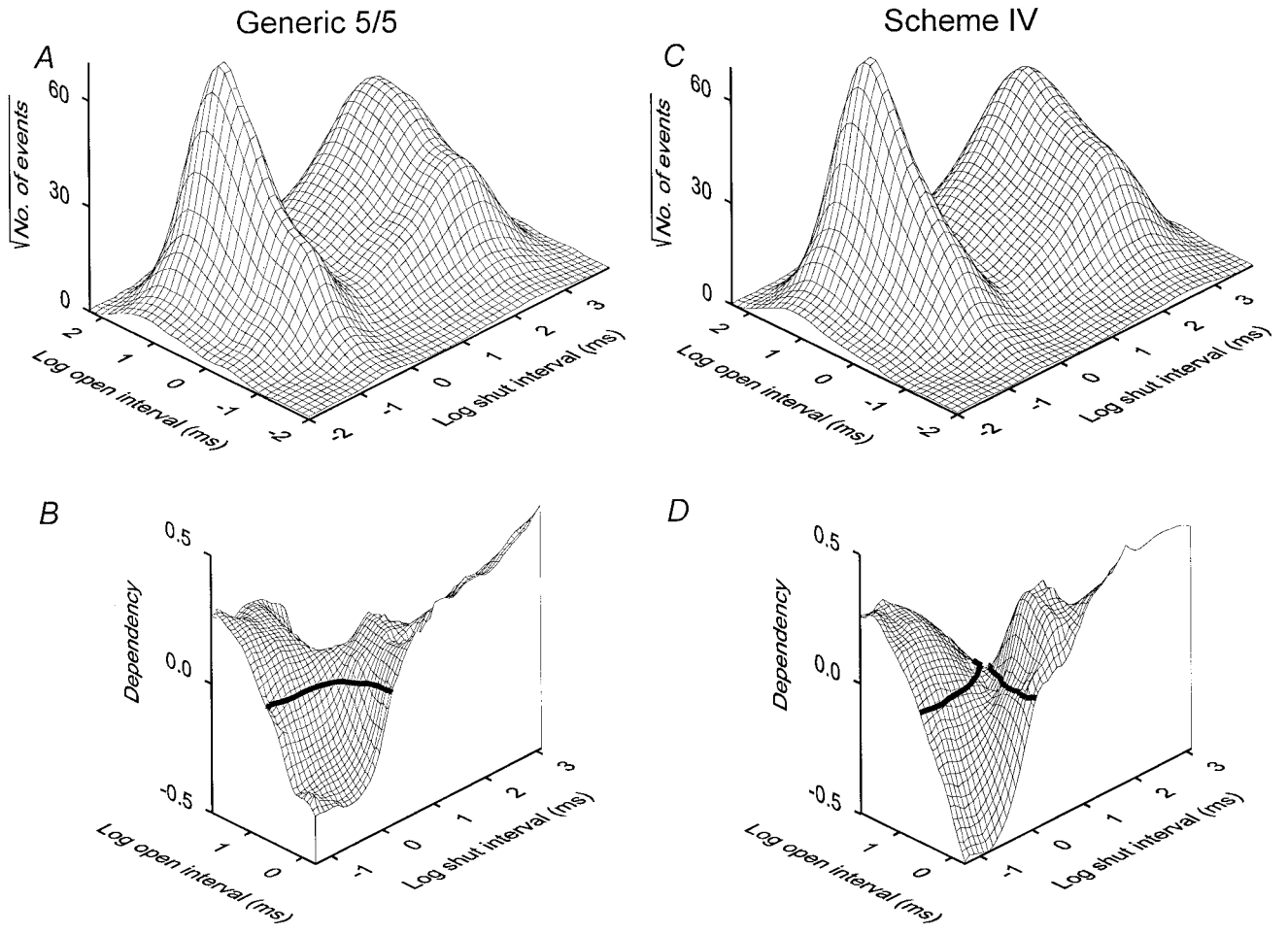

FIGURE 7 The kinetic structure of MS_{xO} channels can be described by both generic and specific models with five open and five closed states. (*A* and *B*) Dwell-time distribution and dependency predicted by a generic gating mechanism with five open and five closed states. (*C* and *D*) Dwell-time distribution and dependency predicted by scheme IV. The rate constants used in the predictions were obtained from the maximum likelihood fitting of the 2-D dwell-time distribution in Fig. 5 *A*. The rate constants for scheme IV were (s^{-1}): k16, 501.0; k61, 0.7400; k27, 18,750; k72, 12890.62; k38, 134.50; k83, 5016; k49, 370.4; k94, 9.970; k5–10, 4396; k10–5, 0.2300; k67, 7.680; k76, 2554; k78, 3034; k87, 2187; k89, 403.6; k98, 15.94; k9–10, 74.40; k10–9, 7.940. Rate constants $<$ 0.001 s^{-1} are not presented. Rate constants are not listed for the generic model, as they have no direct physical meaning. Channel Z100.

open and five closed states should exist that can describe the data as well as the generic model.

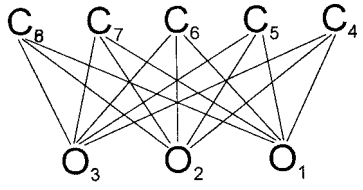

Scheme II

Although scheme II approximated the kinetic structure, the possibility arises that additional states would improve the description of the data, as estimating the numbers of states by fitting with sums of exponential components (as in Fig. 3) indicates only the minimal number of states. To test for additional states, we also fit the data with generic schemes with five open and five closed states (5/5), and six open and six closed states (6/6). The predicted kinetic structures for the 5/5 generic scheme (Fig. 7 *A*, *B*) and the 6/6 generic scheme (not shown) were very similar to that shown in Fig. 6 *C*, *D* for the 3/5 generic scheme. The log likelihood ratios (LLR) of the 5/5 and 3/5 generic schemes to the 6/6 generic scheme for the eight channels are listed in Table 2, indicating some improvement in the description of the data by the 6/6 generic scheme. These results with generic models suggest, then, that gating mechanisms with at least 3–6 open states and 5–6 closed states should be considered for specific models.

Schemes IV and V can account for the steady-state gating of MS_{xO} channels

Based on the observations with generic schemes, we examined some specific models to see if they could serve as

TABLE 2 Log-likelihood ratios, normalized likelihood ratios, and rankings of the indicated schemes determined with 2-D dwell time analysis

Channel	Scheme	LLR*	NLR_{1000}†	R‡	Channel	Scheme	LLR*	NLR_{1000}†	R‡
Z100	Generic 6/6	0.0	1.0		Z108	Generic 6/6	0.0	1.0	
	Generic 5/5	4.47	0.549			Generic 5/5	18.29	0.126	
	Generic 3/5	12.67	0.183			Generic 3/5	20.35	0.100	
	I	87.90	8×10^{-6}	Rej.		I	46.59	0.005	Rej.
	III	41.48	0.004	2		III	58.38	0.001	3
	IV	22.67	0.048	1		IV	22.18	0.081	1
	V	17.53	0.095	3		V	18.39	0.125	2
Z101	Generic 6/6	0.0	1.0		Z112	Generic 6/6	0.0	1.0	
	Generic 5/5	0.84	0.968			Generic 5/5	12.66	0.466	
	Generic 3/5	2.09	0.923			Generic 3/5	14.58	0.415	
	I	17.64	0.510	Rej.		I	34.90	0.122	Rej.
	III	22.66	0.421	2		III	33.94	0.129	1
	IV	2.75	0.900	1		IV	28.76	0.176	2
	V	2.41	0.912	3		V	18.08	0.336	3
Z104	Generic 6/6	0.0	1.0		Z113	Generic 6/6	0.0	1.0	
	Generic 5/5	25.42	0.482			Generic 5/5	3.11	0.770	
	Generic 3/5	100.9	0.055			Generic 3/5	7.72	0.522	
	I	158.8	0.010	Rej.		I	136.7	1×10^{-5}	Rej.
	III	214.4	0.002	3		III	91.26	5×10^{-4}	3
	IV	65.85	0.151	2		IV	3.52	0.744	1
	V	36.79	0.347	1		V	3.29	0.758	2
Z105	Generic 6/6	0.0	1.0		Z114	Generic 6/6	0.0	1.0	
	Generic 5/5	3.05	0.738			Generic 5/5	1.44	0.816	
	Generic 3/5	25.03	0.083			Generic 3/5	2.76	0.677	
	I	63.49	0.002	Rej.		I	53.50	5×10^{-4}	Rej.
	III	68.16	0.001	3		III	32.18	0.010	2
	IV	10.30	0.359	1		IV	9.76	0.251	1
	V	6.11	0.544	2		V	2.59	0.693	3

*LLR is calculated from the log likelihood for the generic 6/6 scheme minus the log likelihood for the indicated scheme.
†NLR_{1000} (Eq. 3 in Methods) is the ratio of the likelihood of the indicated scheme to the likelihood of the generic 6/6 scheme, which was taken to be the theoretical best fit to the two-dimensional distributions.
‡Rankings of the nonsequential specific schemes are based on the Schwarz criterion (Eq. 5 in Methods). Rej. in the ranking column indicates that the scheme was rejected because it did not describe the dependency.

working hypotheses to describe the gating. Three of 19 examined models are indicated by schemes III, IV, and V. In general, specific schemes IV (5/5) and V (6/6) gave somewhat better visual descriptions of the experimental data than specific scheme III (3/5), and the more complex specific schemes also improved the NLR values in Table 2 (to be discussed later). An example is presented in Fig. 7 *C*,*D*, which plots the kinetic structure predicted by scheme IV. Comparison of this predicted kinetic structure to the experimental data in Fig. 5 *A*, *B* and the kinetic structure predicted by the generic 5/5 model in Fig. 7 *A*, *B* indicates that scheme IV described the major features of the data, but not as well as the generic 5/5 model. Predictions from specific scheme V and the generic 6/6 model (both not shown) were just slightly improved over those from scheme IV and the generic 5/5 model.

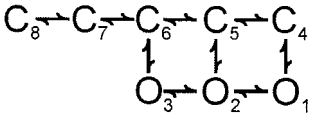

Scheme III

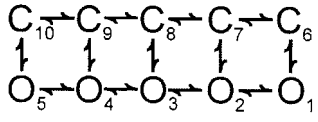

Scheme IV

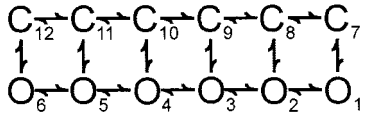

Scheme V

Fig. 8 presents an additional example of data from an MS_{XO} channel obtained under rather different conditions than for the data in the previous figures. Fig. 8 is for

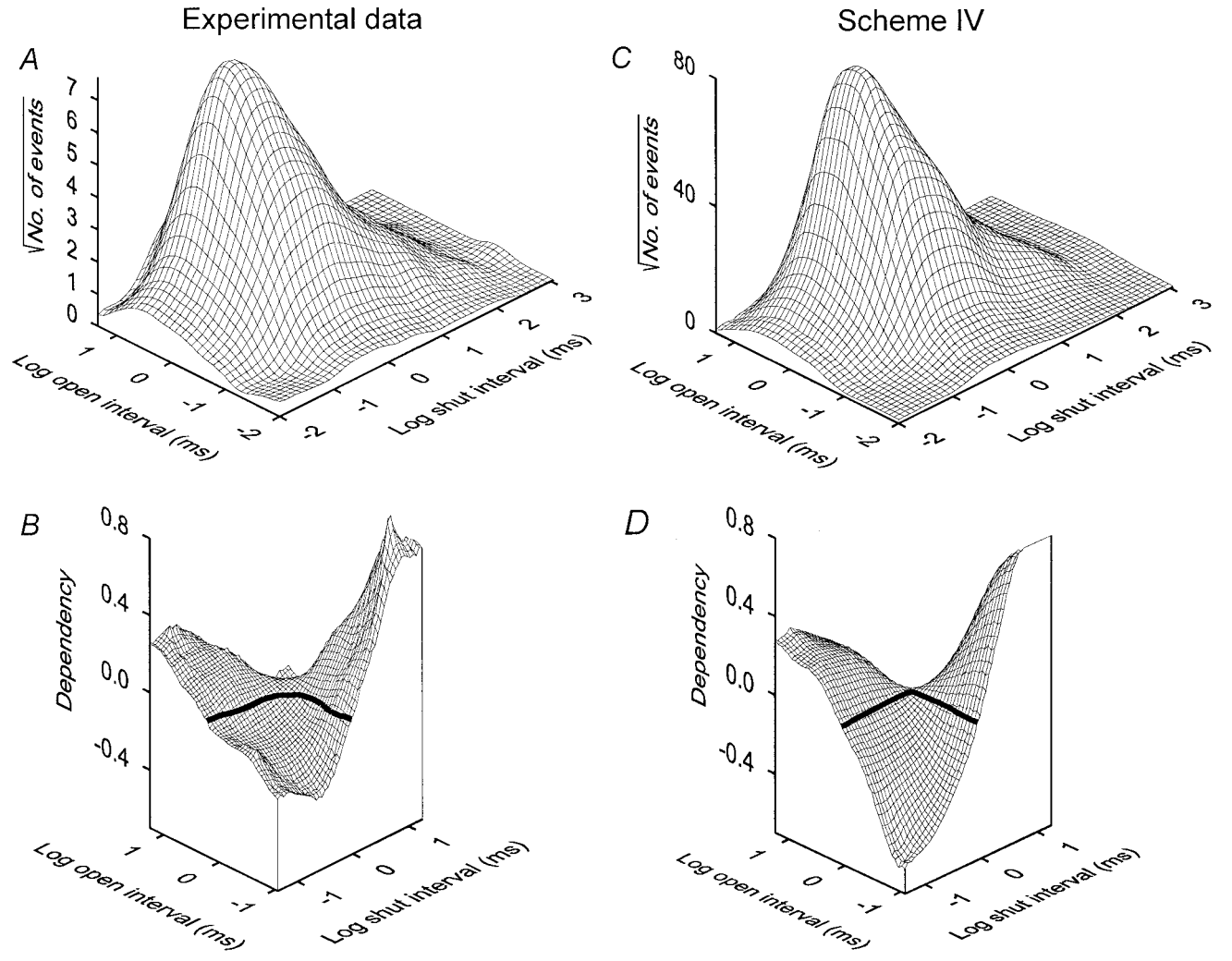

FIGURE 8 Scheme IV can approximate the kinetic structure of MS_{XO} channels activated by depolarization. (*A* and *B*) Dwell-time distribution and dependency plot for a channel activated by holding the membrane potential at −20 mV. (*C* and *D*) Dwell-time distribution and dependency predicted by scheme IV. The rate constants used in the predictions were obtained from the maximum likelihood fitting of the 2-D dwell-time distribution in Fig. 8 *A*. The rate constants for Scheme IV were (s^{-1}): k16, 417.7; k61, 3902; k27, 4665; k72, 205.9; k38, 139.2; k83, 6.550; k49, 441.9; k94, 16.60; k5–10, 118,200; k10–5, 16,330; k67, 1371; k76, 1037; k78, 674.0; k87, 150.4; k89, 68.74; k98, 37.96; k9–10, 1.290; k10–9, 5.560. Rate constants < 0.001 s^{-1} are not presented. Channel Z112.

channel Z112 activated by prolonged depolarization to −20 mV. The predicted kinetic structure shown in Fig. 8 *C*, *D* indicates that scheme IV could also describe the major features of the single-channel activity for this channel activated by depolarization. The description of the higher P_o (0.34) data for channel Z112 in Fig. 8 and the lower P_o (0.07) for channel Z100 in Fig. 5 also shows that scheme IV can describe the data over a range of values of P_o.

Although schemes III–V allow direct transitions between adjacent open states, the estimated rate constants for such transitions of < 0.001 s^{-1}, suggest that few transitions of this type occurred. Consistent with negligible transitions between adjacent open states, eliminating the transition pathways between the open states for schemes III-V typically had little effect on the likelihood estimates. To what extent transition pathways between the open states are a fundamental property of MS channel gating may be revealed when data sets obtained under several different experimental conditions are simultaneously fit. However, we have not yet been able to obtain sufficient stable data over a wide range of pressures to carry out such simultaneous fitting using 2-D dwell-time analysis.

Ranking of models

Although models can be ranked by likelihood to find the most likely model, such rankings do not indicate how well

the top ranked models actually describe the experimental data. Visual comparisons of observed and predicted dwell-time distributions and dependency plots can be used to evaluate whether the top ranked models capture the major features of the data, but such visual comparisons do not indicate whether the top ranked models still give less than ideal descriptions of the data. This problem can be overcome by comparing the likelihood for a model to the likelihood for a theoretical best description of the data. A theoretical best description can be estimated by fitting the data with generic schemes, as the generic schemes should be equivalent to the unknown best model (Rothberg and Magleby, 1998, 1999). For the eight examined channels, a generic scheme with six open and six closed states (generic 6/6) gave better descriptions of the data than generic schemes with five open and five closed states (generic 5/5) or three open and five closed states (generic 3/5). This is indicated in Table 2, which presents the LLR of the generic 6/6 scheme to the other generic schemes. Because the generic 6/6 scheme gave the best description of the data, this description will be considered the theoretical best description for comparison to the descriptions predicted by the various specific kinetic schemes.

Table 2 also presents the LLR of the generic 6/6 scheme to schemes I, III, IV, and V. A LLR of 0 would indicate that a specific scheme describes the data as well as the theoretical best description given by the generic 6/6 scheme. The larger the LLR, the poorer the description. Schemes I, III, IV, and V all gave worse descriptions of the data than the generic 6/6 scheme, so all these specific schemes must be considered too simple. The sequential model described by scheme I can be rejected outright because of the predicted lack of dependency, in contrast to the significant dependence in the data. Schemes III, IV, and V gave increasingly better descriptions of the data, as indicated by the decreasing LLRs to the generic 6/6 scheme. Although schemes III, IV, and V gave worse descriptions of the data than the theoretical best given by the generic 6/6 scheme, the errors associated with these descriptions were small. This can be seen from the NLR_{1000} values in Table 2, which give the ratio of the likelihood for the indicated scheme to the likelihood for the generic 6/6 scheme, normalized to 1000 interval pairs (see Methods). The mean NLR per interval pair, NLR_1, can be calculated from these values to obtain an estimate of the average error per interval pair between the description predicted by the specific scheme when compared with the theoretical best description (see Methods). For the eight channels, the mean values of NLR_1 for Schemes III, IV, and V were 0.995 ± 0.003, 0.998 ± 0.001, and 0.999 ± 0.001, respectively, indicating that the average difference in likelihood per interval pair among schemes III, IV, and V and the theoretical best model was only 0.5%, 0.2%, and 0.1%, respectively.

Schemes III–V have increasing numbers of free parameters because of an increasing number of states and transition pathways among the states. The SC provides a means to rank models with different numbers of free parameters by applying a penalty for each additional free parameter. The rankings of the specific models based on the SC are also presented in Table 2. Scheme IV, with five open and five closed states, was ranked first in 6 of 8 channels, whereas schemes III and V were ranked first for one channel each. Thus, scheme IV can serve as a working hypothesis to describe the gating of MS_{XO} channels.

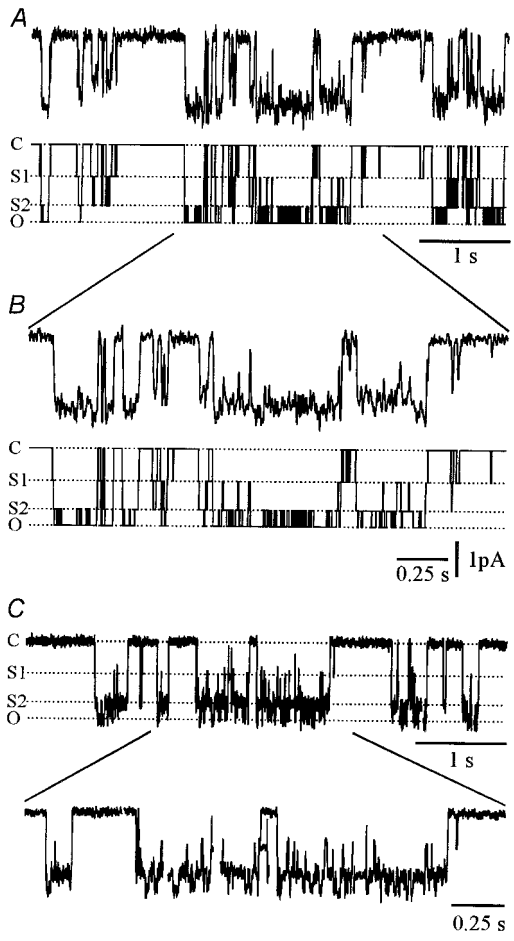

FIGURE 9 MS_{XO} channels gate among at least two subconductance levels (S1 and S2) in addition to the main open level (O). (*A*) Single MS_{XO} channel record (*upper trace*), and the equivalent idealized current trace determined with multiple conductance states analysis (*lower trace*). Downward (inward) currents indicate channel opening. (*B*) Expanded time scale of a region of single-channel records (*upper trace*) and equivalent idealized current trace (*lower trace*). S1 and S2 were 41% and 79% of the main conductance level. Channel Z114, activated by −6 kPa. The idealization traces were produced by segmental k-means (see Methods). (*C*) Single-channel current record predicted by the two-tiered scheme VIII for comparison with the experimental current records in *A* and *B*. The most likely rate constants for channel Z114 for scheme VIII: k12, 307.4; k21, 53.70; k16, 219.0; k61, 1.580; k23, 69.85; k32, 210.1; k25, 11.20; k52, 32.84; k34, 0.3700; k43, 0.4400; k45, 60.39; k54, 49.03; k56, 17,860; k65, 252.0. Simulated single-channel currents were generated using SIMU in the QUB suite (see Methods).

TABLE 3 Log likelihood and rankings of the indicated schemes determined with multiple conductance states analysis

Channel	Scheme	LL	R
Z100	VI	50152	3
	VII	72917	2
	VIII	74059	1
Z101	VI	209393	3
	VII	208974	1
	VIII	208913	2
Z104	VI	−1.08e6	2
	VII	−1.9e6	3
	VIII	1.04e6	1
Z105	VI	99665	3
	VII	245960	2
	VIII	246998	1
Z108	VI	−88401	3
	VII	−87973	2
	VIII	69966	1
Z112	VI	−95449	3
	VII	−62593	2
	VIII	439539	1
Z113	VI	87973	3
	VII	206532	2
	VIII	211902	1
Z114	VI	−68193	3
	VII	2203	2
	VIII	87608	1

Subconductance level analysis also suggests that MS_{XO} channels gate nonsequentially

In the previous sections the kinetic structure and gating mechanism of the MS_{XO} channel was probed by measuring interval durations with half-amplitude threshold analysis. When 50% threshold analysis is used to detect opening and closing of the channel (see Methods), subconductance open levels with amplitudes >50% of the full open level are classified as fully open and could add components to the open time-distributions. Conversely, subconductance levels with amplitudes <50% would be detected as closed intervals and could add components to the closed time-distributions. Because MS_{XO} channels also display subconductance levels (Methfessel et al., 1986; Lane et al., 1991; Silberberg and Magleby, 1997), some of the states in the various schemes we have considered may represent subconductance states. Nevertheless, the correlation that was observed between the measured adjacent open and closed intervals suggests that the gating of MS_{XO} is not strictly sequential from closed to open, but involves two or more gateway states (independent transition pathways) between the open and closed states.

This nonsequential gating mechanism for MS_{XO} channels differs from that for a MS channel in bacteria, MScL, where the gating is described by a model in which the channel moves sequentially from a fully closed state through three subconductance open states to a fully open state (Sukharev et al., 1999a). To rule out the possibility that the apparent difference in gating of MS_{XO} and MScL channels is attributable to the different analysis techniques used for each channel (half-amplitude threshold detection and 2-D dwell-time analysis vs. subconductance level analysis, respectively), we investigated whether an analysis of MS_{XO} channels that allows transitions to subconductance levels is also consistent with nonsequential gating.

Close examination of the single-channel records of the eight MS_{XO} channels investigated in this study revealed that the channels gate among multiple conductance states. The amplitude of the subconductance states was estimated with the segmental k-means algorithm (Qin et al., 1996), which was also used to generate idealized conductance-state sequences. A typical single-channel record and its idealized current trace are shown in Fig. 9 *A*, *B*, for channel Z114, activated by negative pressure in the pipette. Three open channel current levels were clearly resolved: a main open level (*O*), and two subconductance levels, *S*1 and *S*2, at 41% and 79% of the main open level, respectively (Fig. 9 *A*, *B*).

*S*1 was the most variable among the channels, ranging from 23% to 69% of the main conductance level with a mean (±SE) of 44 ± 6%. *S*2 ranged from 51% to 85% of the main conductance level with a mean (±SE) of 76 ± 4%. Attempting to idealize the data with >3 conducting levels resulted in the detection of additional subconductance levels of <10% of the main open level, which was within the noise of the closed level. Thus, all subsequent analysis assumed the channels gate among one or more closed states and three conducting (open) states.

The number of closed states cannot be determined directly from the number of current levels because all nonconducting states (closed states) have the same zero conductance. Hence, each of the eight channels was first fit with all possible nonlooping models containing just one closed state, two subconductance states, and one main open state (1/3 models). These models were then ranked according to the LLR to identify which of the kinetic models best described the gating of MS_{XO} channels. Of all possible 1/3 models, 7 of 8 channels were best fit with the linear model given by scheme VI, in which the closed state (C), the two subconductance states (S1 and S2), and the main conducting state (O) are in sequence.

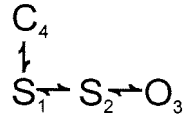

Scheme VI

Because the half-amplitude threshold analysis in the previous sections indicated multiple closed states, the channels were then fit with a linear model containing three closed states in sequence preceding the two subconductance states, S1 and S2, followed by the open state (3/3 model). This sequential model, given by scheme VII, ranked above scheme VI for 7 of the 8 channels using the SC given by Eq. 5 in Methods.

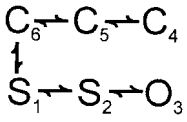

Scheme VII

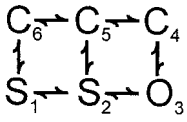

Scheme VIII

Based on the results obtained with the 2-D dwell-time analysis, in which scheme IV typically ranked highest, we then fit the data with a 3/3 model that has multiple gateway states, similar to scheme IV. In this model, the two subconductance states and the fully open state were each directly connected to a different closed state, giving three gateway states (scheme VIII). For 7 of the 8 channels, scheme VIII was ranked above schemes VI or VII. This is shown in Table 3, which summarizes the log likelihood values and rankings for schemes VI, VII, and VIII for the eight examined channels. Fig. 9 *C* shows simulated single-channel current records generated using the most likely rate constants for channel Z114 for scheme VIII. The similarity to the actual current records shown in Fig. 9 *A*, *B* is apparent. Although scheme VIII was limited to six states by the resolution of the sublevel analysis, it would be expected from the increased numbers of states detected with 50% threshold analysis that scheme VIII will have to be extended to include additional open and/or subconductance states and also additional closed states.

The results using subconductance level analysis obtained in this section are in agreement with those using half-amplitude threshold analysis obtained in previous sections: MS_{XO} channels gate nonsequentially with multiple gateway states. Visual inspection of both the experimental and idealized single-channel current records is consistent with this conclusion, as there seem to be occasional direct transitions between the closed level and each of the three open levels (Fig. 9 *A*, *B*). Thus, the apparent difference in gating mechanism between MS_{XO} channels and MScL channels is not a result of the method of analysis.

DISCUSSION

The purpose of the present study was to investigate the steady state gating of MS channels in *Xenopus* oocytes (MS_{XO} channels). Although we studied these channels in excised patches of membrane using the patch-clamp technique, it has recently been shown that these channels can also be activated in intact oocytes in response to mechanical stimulation (Saito et al., 2000; Zhang and Hamill, 2000a,b). We found that the 1-D open and closed dwell-time distributions were typically described by three open and five closed significant exponential components, suggesting that the channel typically enters a minimum of three open and five closed states during steady-state gating. Dependency and dependency significance plots revealed that the durations of adjacent open and closed intervals were significantly correlated, indicating that all sequential (linear) gating mechanisms with a single gateway state can be rejected outright for the gating of MS_{XO} channels. This conclusion was corroborated by subconductance level analysis.

Kinetic gating mechanisms with 3–6 open states and 5–6 closed states were fit to 2-D dwell-time distributions to estimate the most likely rate constants for each scheme. The considered gating mechanisms were then ranked using the likelihood tests that apply a penalty for additional free parameters. Minimal kinetic models, as developed here, give information about the minimal numbers of conformations the channel typically entered during gating. More complex conformational models could also give rise to the same minimal kinetic models in the case that some of the conformational states were entered infrequently or resulted in components with overlapping time constants. The top ranked model, scheme IV, which could account for the major features of the single-channel data, was a two-tiered gating mechanism with five closed and five open states, with each closed state being directly connected to an open state. Adding an additional open and closed state to scheme IV to obtain scheme V improved the description of the data, but not significantly.

Although the molecular structure of MS_{XO} is not yet known, it is of interest to consider what types of physical models might be consistent with the kinetic models. The 10-state, two-tiered model described by scheme IV would be kinetically consistent with a channel comprising at least four subunits, in which each subunit can exist in at least two conformations, the movement of the subunits is not strictly coupled, and that the opening and closing conformation is separate from the subunit conformations. Examples of cartoons of such a four-subunit model are presented in Fig. 10 of McCormack et al. (1994) and scheme XV in Rothberg and Magleby (1999). On the same basis, the 12-state, two-tiered model (scheme V) would be consistent with a channel comprising at least five subunits, as has been reported for

the subunit structure of a homolog of MScL from *Mycobacterium tuberculosis* (Chang et al., 1998) and of MScL of *E. coli* (Sukharev et al., 1999b, 2001). Other physical models are, of course, possible, and detailed studies on other channel types suggest that the gating could be far more complex (Zagotta et al., 1994; Zheng and Sigworth, 1998).

Activation of MS_{XO} channels by voltage

The steady-state activity of MS_{XO} channels increases with membrane depolarization (Methfessel et al. 1986; Silberberg and Magleby, 1997), and this depolarization-induced increase in activity also occurs in the presence of applied stretch (Yang and Sachs, 1990). We have recently observed that depolarization of membrane patches in borosilicate glass pipettes induces displacement of the membrane patch into the patch pipette, and that the displacement is associated with activation of the MS_{XO} channels in the patch, presumably through displacement-associated increases in membrane (or cytoskeletal) tension (Gil et al., 1999a,b). If depolarization activates MS_{XO} channels solely through an increase in membrane tension, then activation by voltage or by pressure should have the same effects on the gating, and the kinetic structure of MS_{XO} channels activated by either tension or by depolarization would be the same.

In the present study, 4 of the 8 channels examined in detail were activated by pressure, and 4 were activated by depolarization (Table 1). The major features of the kinetic structure, as revealed by the 2-D dwell-time distributions and the dependency plots, were generally similar for activation by pressure or depolarization. Consistent with this similarity, schemes V and IV gave the first and second best likelihood values, respectively, for all eight channels, whether activated by pressure or by depolarization. When a penalty for free parameters was applied, scheme IV was top ranked for the four channels activated by pressure and for two of the four channels activated by depolarization. These observations are generally consistent with the hypothesis that activation of MS_{XO} channels by voltage occurs through changes in membrane tension, but they are not sufficient to exclude that voltage may also have some additional effects.

Comparison to previous studies on MS_{XO} channels

Yang and Sachs (1990) examined the pressure and voltage dependence of MS_{XO} channels in on-cell patches. The distributions of open and closed times suggested 1–2 open states and three closed states. The greater numbers of states detected in our study (2–3 open and 5–7 closed) may reflect a greater number of analyzed intervals together with the use of maximum likelihood fitting, both of which facilitate the detection of exponential components (McManus and Magleby, 1988). Yang and Sachs (1990) used sequential models with three closed and one open state (C4-C3-C2-O1 or C4-C3-O1-C2) to characterize the effects of pressure and voltage on gating. The major effect of increasing pressure was to increase the rate constants driving the gating toward the open state away from the long (C4) and intermediate (C3) duration closed states. The major effects of depolarization and pressure on the rate constants in the study of Yang and Sachs (1990) were similar, consistent with the possibility that depolarization may act through increases in tension (Gil et al., 1999b).

Although the four-state sequential models used by Yang and Sachs (1990) captured the general features of the 2-D dwell-time distributions, both models would generate dependency plots that are essentially flat, in contrast to the significant dependencies of the experimental data (Fig. 5). Thus, the models of Yang and Sachs (1990) would have to be expanded to include additional states and transition pathways between open and closed states to account for the increased numbers of components and correlation information revealed by the 2-D analysis, and to account for the observed multiple conductance levels (Fig. 9). Such expansion of complexity with increasing resolution of analysis is a common feature of kinetic studies and is to be expected.

Comparison to some other MS channels

In their initial landmark studies, Guharay and Sachs (1984, 1985) first described and characterized single MS channels. Kinetic analysis of the single-channel currents in patches of membrane from tissue-cultured embryonic chick skeletal muscle indicated at least three closed states and one open state. The gating of the channels was modeled using the four state sequential kinetic scheme, C-C-C-O. A sequential kinetic scheme, C-C-O, has also been used to characterize MS channels from amphibian proximal tubule (Sackin, 1995). For both schemes, the MS rate constant was the transition leaving the longest (leftmost) closed state. The above-mentioned channels were not investigated with either correlation analysis or subconductance analysis. Hence, it is possible that the apparent simpler schemes for these MS channels when compared with those revealed in the present study reflect, at least to some extent, differences in the resolution of the analysis.

Because MS channels in eukaryotes seem to require coupling to membrane-associated structures (extracellular matrix and/or cytoskeleton) for stretch activation (Sachs and Morris, 1998), it also cannot be excluded that some differences in gating might arise from differences in the membrane-associated structures or in the coupling. Further, because the above-mentioned MS channels have not yet been cloned, it is not known whether differences in structure contribute to the differences in gating, as various MS channels can have different structures. For example, the large conductance MS channel from *E. coli*, MScL (Sukharev et al., 1994, 2001), exhibits little structural similarity to the

cloned yeast MS channels (Iida et al. 1994; Kanzaki et al., 1999), or to the *Caenorhabditis elegans* degenerin UNC-105, implicated in mechanotransduction (Garcia-Anoveros et al., 1998), or to the mammalian sodium channel BNC1 associated with normal touch sensation (Price et al., 2000).

Models consistent with the gating of MScL channels are markedly different from those considered here for MS_{XO} channels. MScL channels gate among a single closed state and four open states of different conductance (Sukharev et al., 1999a). The three subconductance levels of the MScL channel are at ~30, 70, and 90% of the fully open state, with the transition between the closed state and the lowest conducting open state the most sensitive to tension. MScL channel gating was described by a sequential model in which the open states were in series of increasing conductance, and the closed state was directly connected to the lowest conductance open state. A structural model for MScL with sequential conformational changes has been developed that is consistent with the single-channel data (Sukharev et al., 2001). In contrast, the present study suggests that each of the conducting states of the MS_{XO} channel is directly connected to a closed state, in addition to being connected sequentially to one another.

The actual differences in gating mechanism may not be as profound as suggested by the differences in the models. Many of the transitions between the fully closed and the fully open states in the single-channel records for the MScL channel seem to occur in one step (Sukharev et al., 1999a, 2001), as if sequential transitions through the substates are either not always required for transitions between the open and closed states or occur so rapidly that they are not apparent. Both one-step transitions (C4-O3 in scheme VIII) and also sequential transitions (C6-S1-S2-O3 in scheme VIII) can occur in the models used to describe the gating of MS_{XO} channels. Consequently, it would be useful to investigate whether the gating of other MS channels, such as MScL, is consistent with gating mechanisms with multiple gateway states, as was found for MS_{XO} channels.

Supported in part by grant 93–00061 from the US-Israel Binational Science Foundation and by the Zlotowski Center for Neuroscience (to S.D.S) and grant AR 32805 from the National Institutes of Health and a grant from the Muscular Dystrophy Association (to K.L.M.). Z.G. is a recipient of the Kreitman, Folks, and Landau Doctoral Fellowships.

REFERENCES

Blatz, A. L., and K. L. Magleby. 1986a. Correcting single channel data for missed events. *Biophys. J.* 49:967–980.

Blatz, A. L., and K. L. Magleby. 1986b. Quantitative description of three modes of activity of fast chloride channels from rat skeletal muscle. *J. Physiol.* 378:141–174.

Chang, G., R. H. Spencer, A. T. Lee, M. T. Barclay, and D. C. Rees. 1998. Structure of the MscL homolog from *Mycobacterium* tuberculosis: a gated mechanosensitive ion channel. *Science.* 282:2220–2226.

Colquhoun, D., and A. G. Hawkes. 1981. On the stochastic properties of single ion channels. *Proc. R. Soc. Lond. Biol.* 211:205–235.

Colquhoun, D., and A. G. Hawkes. 1982. On the stochastic properties of bursts of single ion channel openings and clusters of bursts. *Phil. Trans. R. Soc. Lond. B. Biol. Sci.* 300:1–59.

Colquhoun, D., and A. G. Hawkes. 1987. A note on correlations in single ion channel records. *Proc. R. Soc. Lond. B.* 230:15–52.

Colquhoun, D., A. G. Hawkes, and K. Srodzinski. 1996. Joint distributions of apparent open and shut times of single-ion channels and maximum likelihood fitting of mechanisms. *Phil. Trans. R. Soc. Lond. A.*2555–2590.:

Colquhoun, D., and F. J. Sigworth. 1995. Fitting and statistical analysis of single-channel records. *In* Single-Channel Recording. B. Sakmann and E. Neher, editors. Plenum Press, New York. 483–587.

Crouzy, S. C., and F. J. Sigworth. 1990. Yet another approach to the dwell-time omission problem of single-channel analysis. *Biophys. J.* 58:731–743.

Delcour, A. H., Lipscombe, D., and R. W. Tsien. 1993. Multiple modes of *N*-type calcium channel activity distinguished by differences in gating kinetics. *J. Neurosci.* 13:181–194.

Fredkin, D. R., M. Montal, and J. A. Rice. 1985. Identification of aggregated Markovian models: application to the nicotinic acetylcholine receptor. *In* Proceedings of the Berkeley Conference in Honor of Jerzy Neyman and Jack Kiefer. L. M. LeCam and R. A. Olshen, editors. Wadsworth Press, Belmont. 269–289.

Garcia-Anoveros, J., J. A. Garcia, J. D. Liu., and D. P. Corey. 1998. The nematode degenerin UNC-105 forms ion channels that are activated by degeneration- or hypercontraction-causing mutations. *Neuron.* 20: 1231–1241.

Gil, Z., K. L. Magleby, and S. D. Silberberg. 1999a. Membrane-pipette interactions underlie delayed voltage activation of mechanosensitive channels in *Xenopus* oocytes. *Biophys. J.* 76:3118–3127.

Gil, Z., S. D. Silberberg, and K. L. Magleby. 1999b. Voltage-induced membrane displacement in patch pipettes activates mechanosensitive channels. *Proc. Natl. Acad. Sci. U.S.A.* 96:14594–14599.

Guharay, F., and F. Sachs. 1984. Stretch-activated single ion channel currents in tissue-cultured embryonic chick skeletal muscle. *J. Physiol.* 352:685–701.

Guharay, F., and F. Sachs. 1985. Mechanotransducer ion channels in chick skeletal muscle: the effects of extracellular pH. *J. Physiol.* 363:119–134.

Gustin, M. C., X. L. Zhou, B. Martinac, and C. Kung. 1988. A mechanosensitive ion channel in the yeast plasma membrane. *Science.* 242: 762–765.

Hamill, O. P., A. Marty, E. Neher, B. Sakmann, and F. J. Sigworth. 1981. Improved patch-clamp techniques for high-resolution current recording from cells and cell-free membrane patches. *Pflügers Arch.* 391:85–100.

Hamill, O. P., and D. W. McBride, Jr. 1992. Rapid adaptation of single mechanosensitive channels in *Xenopus* oocytes. *Proc. Natl. Acad. Sci. U.S.A.* 89:7462–7466.

Hamill, O. P., and D. W. McBride, Jr. 1996. The pharmacology of mechanogated membrane ion channels. *Pharmacol. Rev.* 48:231–252.

Hess, P., J. B. Lansman, and R. W. Tsien. 1984. Different modes of Ca channel gating behaviour favoured by dihydropyridine Ca agonists and antagonists. *Nature.* 311:538–544.

Iida, H., H. Nakamura, T. Ono, M. S. Okumura, and Y. Anraku. 1994. *MID1*, a novel *Saccharomyces cerevisiae* gene encoding a plasma membrane protein, is required for Ca^{2+} influx and mating. *Mol. Cell. Biol.* 14:8259–8271.

Kanzaki. M., M. Nagasawa, I. Kojima, C. Sato, K. Naruse, M. Sokabe, and H. Iida. 1999. Molecular identification of a Eukaryotic, stretch-activated nonselective cation channel. *Science.* 285:882–886.

Keller, B. U., M. S. Montal, R. P. Hartshorne, and M. Montal. 1990. Two-dimensional probability density analysis of singe channel currents from reconstituted acetylcholine receptors and sodium channels. *Arch. Biochem. Biophys.* 276:47–54.

Kienker, P. 1989. Evidence of aggregated Markov models of ion-channel gating. *Proc. R. Soc. Lond. B. Biol. Sci.* 236:269–309.

Lane, J. W., D. W. McBride, and O. P. Hamill. 1991. Amiloride block of the mechanosensitive cation channel in *Xenopus* oocytes. *J. Physiol.* 441:347–366.

Le Dain, A. C., N. Saint, A. Kloda, A. Ghazi, and B. Martinac. 1998. Mechanosensitive ion channels of the archaeon *Haloferax volcanii*. *J. Biol. Chem.* 273:12116–12119.

Magleby, K. L., and B. S. Pallotta. 1983. Burst kinetics of single calcium-activated potassium channels in cultured rat skeletal muscle. *J. Physiol.* 344:605–623.

Magleby, K. L., and L. Song. 1992. Dependency plots suggest the kinetic structure of ion channels. *Proc. R. Soc. Lond. B Biol. Sci.* 249:133–142.

McCormack, K., W. J. Joiner, and S. H. Heinemann. 1994. A characterization of the activating structural rearrangements in voltage-dependent *Shaker* K^+ channels. *Neuron* 12:301–315.

McManus, O. B., and K. L. Magleby. 1988. Kinetic states and modes of single large-conductance calcium-activated potassium channels in cultured rat skeletal muscle. *J. Physiol.* 402:79–120.

McManus, O. B., and K. L. Magleby. 1991. Accounting for the Ca^{2+}-dependent kinetics of single large-conductance Ca^{2+}-activated K^+ channels in rat skeletal muscle. *J. Physiol.* 443:739–777.

Methfessel, C., V. Witzemann, T. Takahashi, M. Mishina, S. Suma, and B. Sakmann. 1986. Patch clamp measurements on *Xenopus laevis* oocytes: currents through endogenous channels and implanted acetylcholine receptor and sodium channels. *Pflügers Arch.* 407:577–588.

Morris, C. E. 1990. Mechanosensitive ion channels. *J. Membr. Biol.* 113:93–107.

Oakley, A. J., Martinac, B., and M. C. Wilce. 1999. Structure and function of the bacterial mechanosensitive channel of large conductance. *Protein Sci.* 8:1915–1921.

Patlak, J. B., K. A. F. Gration, and P. R. N. Usherwood. 1979. Single glutamate-activated channels in locust muscle. *Nature.* 278:643–645.

Patlak, J. B., and M. Ortiz. 1985. Slow currents through single sodium channels of the adult rat heart. *J. Gen. Physiol.* 86:89–104.

Price, M. P., G. R. Lewin, S. L. Mcllwrath, C. Cheng, J. Xie, P. A. Heppenstall, C. L. Stucky, A. G. Mannsfeldt, T. J. Brennan, H. A. Drummond, J. Qiao, C. J. Benson, D. E. Tarr, R. F. Hrstka, B. Yang, R. A. Williamson, and M. J. Welsh. 2000. The mammalian sodium channel BNC1 is required for normal touch sensation. *Nature.* 407: 1007–1011.

Qin, F., A. Auerbach, and F. Sachs. 1996. Estimating single-channel kinetic parameters from idealized patch-clamp data containing missed events. *Biophys. J.* 70:264–280.

Qin, F., A. Auerbach, and F. Sachs. 2000a. A direct optimization approach to hidden Markov modeling for single channel kinetics. *Biophys. J.* 79:1915–1927.

Qin, F., A. Auerbach, and F. Sachs. 2000b. Hidden Markov modeling for single channel kinetics with filtering and correlated noise. *Biophys. J.* 79:1928–1944.

Rothberg, B. S., R. A. Bello, and K. L. Magleby. 1997. Two-dimensional components and hidden dependencies provide insight into ion channel gating mechanisms. *Biophys. J.* 72:2524–2544.

Rothberg, B. S., and K. L. Magleby. 1998. Kinetic Structure of large-conductance Ca^{2+}-activated K^+ channels suggests that the gating includes transitions through intermediate or secondary states: a mechanism for flickers. *J. Gen. Physiol.* 111:751–780.

Rothberg, B. S., and K. L. Magleby. 1999. Gating kinetics of single large-conductance Ca^{2+}-activated K^+ channels in high Ca^{2+} suggest a two-tiered allosteric gating mechanism. *J. Gen. Physiol.* 114:93–124.

Sachs, F., and C. E. Morris. 1998. Mechanosensitive ion channels in nonspecialized cells. *In* Reviews of Physiology and Biochemistry and Pharmacology. M. P. Blaustein, R. Greger, H. Grunicke, R. Jahn, L. M. Mendell, A. Miyajima, D. Pette, G. Schultz, and M. Schweiger, editors. Springer-Verlag, Berlin.1–78.

Sackin, H. 1989. Stretch-activated potassium channel sensitive to cell volume. *Proc. Natl. Acad. Sci. U.S.A.* 86:1731–1735.

Sackin, H. 1995. Mechanosensitive channels. *Annu. Rev. Physiol.* 57: 333–353.

Saito, T., T. Ishikawa, K. Obara, and K. Nakayama. 2000. Characterization of whole-cell currents elicited by mechanical stimulation of *Xenopus* oocytes. *Pflügers Arch.* 440:858–865.

Sakmann, B., and E. Neher. 1995. Single Channel Recording. Plenum Press, New York.

Schwarz, G. 1978. Estimating the dimension of a model. *Ann. Statistics.* 6:461–464.

Sigworth, F. J., and S. M. Sine. 1987. Data transformations for improved display and fitting of single-channel dwell time histograms. *Biophys. J.* 52:1047–1054.

Silberberg, S. D., and K. L. Magleby. 1997. Voltage-induced slow activation and deactivation of mechanosensitive channels in *Xenopus* oocytes. *J. Physiol.* 505:551–569.

Sokabe, M., F. Sachs, and Z. Jing. 1991. Quantitative video microscopy of patch clamped membranes stress, strain, capacitance, and stretch channel activation. *Biophys. J.* 59:722–728.

Stühmer, W., and A. B. Parekh. 1995. Electrophysiological recordings from *Xenopus* oocytes. *In* Single-Channel Recording. B. Sakmann and E. Neher, editors. Plenum Press, New York. 341–356.

Sukharev, S. I., P. Blount, B. Martinac, F. R. Blattner, and C. Kung. 1994. A large-conductance mechanosensitive channel in *E. coli* encoded by mscL alone. *Nature.* 368:265–268.

Sukharev, S. I., W. J. Sigurdson, C. Kung, and F. Sachs. 1999a. Energetic and spatial parameters for gating of the bacterial large conductance mechanosensitive channel, MscL. *J. Gen. Physiol.* 113:525–539.

Sukharev, S. I., M. J. Schroeder, and D. R. McCaslin. 1999b. Stoichiometry of the large conductance bacterial mechanosensitive channel of *E. Coli*. A biochemical study. *J. Membrane Biol.* 171:183–193.

Sukharev, S., M. Betanzos, C. S. Chiang, and H. R. Guy. 2001. The gating mechanism of the large mechanosensitive channel MscL. *Nature.* 409: 720–724.

Yang, X-C., and F. Sachs. 1990. Characterization of stretch-activated ion channels in *Xenopus* oocytes. *J. Physiol.* 431:103–122.

Zagotta, W. N., T. Hoshi, and R. W. Aldrich. 1994. Shaker potassium channel gating. III: Evaluation of kinetic models for activation. *J. Gen. Physiol.* 103:321–362.

Zhang, Y., and O. P. Hamill. 2000a. Calcium-, voltage- and osmotic stress-sensitive currents in *Xenopus* oocytes and their relationship to single mechanically gated channels. *J. Physiol.* 523:83–99.

Zhang, Y., and O. P. Hamill. 2000b. On the discrepancy between whole-cell and membrane patch mechanosensitivity in *Xenopus* oocytes. *J. Physiol.* 523:101–115.

Zheng, J., and F. J. Sigworth. 1998. Intermediate conductances during deactivation of heteromultimeric potassium channels. *J. Gen. Physiol.* 110:101–117.